

# Designing Marshall positive $SU(N)$ quantum spin Hamiltonians

Ribhu K. Kaul

*Department of Physics & Astronomy, University of Kentucky, Lexington, KY-40506-0055*

We consider bipartite  $SU(N)$  spin Hamiltonians with a fundamental representation on one sublattice and a conjugate to fundamental on the other sublattice. By mapping these antiferromagnets to certain classical loop models in one higher dimension, we provide a practical strategy to write down a large family of  $SU(N)$  symmetric spin Hamiltonians that satisfy Marshall's sign condition. This family includes all previously known sign-free  $SU(N)$  spin models and in addition provides a large set of new models that can be studied efficiently with quantum Monte Carlo methods. As an application of our idea to the square lattice, we show that in addition to Sandvik's  $Q$ -term, there is an independent non-trivial four-spin  $R$ -term that is sign-free. Using numerical simulations, we show how the  $R$ -term provides a new route to the study of quantum criticality of Néel order.

The study of the ground states of lattice spin Hamiltonians has a long history in physics [1]. Due to its relevance to quantum magnetism in solid state materials, the study is currently one of the cornerstones of modern condensed matter physics [2]. The scarcity of controlled analytic solutions of spin models has spurred the development of a wide array of sophisticated numerical approaches [3–5]. Quantum Monte Carlo (QMC) is often the method of choice for unbiased studies of large higher dimensional ( $d > 1$ ) quantum spin systems [6]. In practice this capability is restricted to models that do not suffer from the notorious sign-problem [7, 8]. The absence of this problem is guaranteed in standard world line methods only if the Marshall sign rule [9] ( $\langle \alpha | H | \beta \rangle < 0$  for  $\alpha \neq \beta$ ) is satisfied in a convenient local basis. Surprisingly, at the current time, there is no systematic knowledge of the extent of Marshall-positive spin Hamiltonians. Such an understanding would clearly be of great practical and conceptual value, since Marshall-positive Hamiltonians constitute a large fraction of the valuable examples of higher-dimensional models that can be simulated on a classical computer in polynomial time [10, 11].

Here we will address this issue for a specific but important subset of models,  $SU(N)$  quantum spin Hamiltonians on the square lattice, which have spins that transform as the fundamental representation ( $\mathcal{N}$ ) on the A sublattice and the conjugate to fundamental ( $\bar{\mathcal{N}}$ ) on the B sublattice, Fig. 1(a) [12]. Let us call the set of all such Hamiltonians  $\mathcal{N}\text{-}\bar{\mathcal{N}}$ . Note that for  $N = 2$  the fundamental representation is self-conjugate so this class includes all  $SU(2)$  symmetric Hamiltonians.  $\mathcal{N}\text{-}\bar{\mathcal{N}}$  includes both models that are widely believed to have no solution to the sign problem (e.g. the  $J_1$ - $J_2$  Heisenberg model with  $J_1, J_2$  anti-ferro [13]) and others for which the absence of the sign problem is well known. The simplest interaction in  $\mathcal{N}\text{-}\bar{\mathcal{N}}$  was introduced by Affleck [12],

$$H_{J_1}^{(N)} = -J_1 T_i^a \cdot T_j^{a*}, \quad (1)$$

where  $i$  and  $j$  are on different sublattices of the bipartition and  $T^a$  are the  $SU(N)$  generators in the fundamental representation (sum on  $a$  is implied). It happens that this

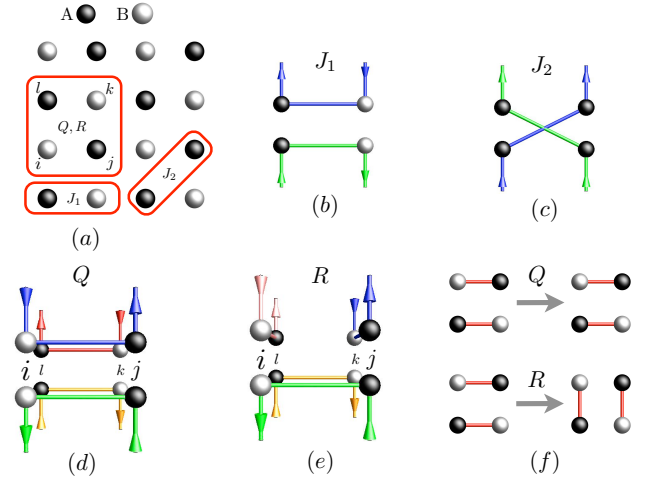


FIG. 1. Cartoon illustration of the various Marshall positive interaction terms studied in the paper. (a) shows the decomposition of the bipartite square lattice into A and B sublattices, and the groups of sites that the various interactions act on. (b-e) cartoons of the different interactions acting on the basis states, the initial state is shown at the bottom and the final state is shown on top. (b) shows the  $J_1$  interaction that acts between sites on different sublattices. (c) shows the  $J_2$  interaction that acts on sites on the same sublattice. (d) shows an example of a  $Q$  interaction and (e) shows an example of an  $R$  interaction that both act on elementary plaquettes of the square lattice. Colors of the loop represent the  $N$  colors of  $SU(N)$ . Note that loops meeting at a vertex may have the same color and that the loops always travel up on opposite directions on the A and B sublattices. (f) Cartoon illustration of singlet rearrangements effected by  $R$  and  $Q$  terms, see discussion on Eq. (5).

interaction is Marshall positive and can hence be simulated efficiently with QMC [14]. We note that the familiar  $SU(2)$  Heisenberg antiferromagnet,  $H_{J_1}^{(2)} = J_1 \vec{S}_i \cdot \vec{S}_j$ , a special case of Eq. (1) with  $N = 2$ , was the original model for which Marshall proved his theorem [15]. This fact has been exploited to study it using QMC on various ordered and disordered bipartite lattices for the last three decades (see references in [6]). In an important

breakthrough, Sandvik found that in addition to the two spin interactions, a four-spin plaquette  $Q$ -term [16],

$$H_Q^{(2)} = -Q \left( \vec{S}_i \cdot \vec{S}_j - \frac{1}{4} \right) \left( \vec{S}_k \cdot \vec{S}_l - \frac{1}{4} \right) + i \leftrightarrow k, \quad (2)$$

also satisfied Marshall sign condition (see Fig. 1(a) for site labeling). The sign-free  $J_1$ - $Q$  hamiltonian has since been studied extensively using QMC [17–21]. The discovery of the  $Q$ -idea has lead to the proposal and study of a number of extensions, including generalizations for  $N > 2$  along the lines of Eq. (1) [22–27]. The discovery of the  $Q$ -term and its popularity in numerical studies begs the questions: Are there other  $\mathcal{N}$ - $\tilde{\mathcal{N}}$  models that satisfy Marshall’s sign rule? What is the full extent of these sign-free models?

*General sign free  $\mathcal{N}$ - $\tilde{\mathcal{N}}$  models:* We now show that it is easiest to address these questions by considering the structure of the imaginary time statistical mechanics ( $Z = \text{Tr}[e^{-\beta H}]$ ) generated by the  $\mathcal{N}$ - $\tilde{\mathcal{N}}$  Hamiltonians. Each site on the bipartite lattice has  $N$  states. Our goal is to write down sign-positive model interactions that are invariant under rotation by  $U$  (an  $\text{SU}(N)$  matrix) on all the A sublattice spins and rotation  $U^*$  on all the B sublattice spins. Let us begin by reviewing how this works for a two-spin interaction, which we can write in the form  $\Gamma_{\alpha\beta\gamma\eta} |\alpha\beta\rangle \langle \gamma\eta|$ . To preserve  $\text{SU}(N)$  invariance, the spin indices on the sites have to be paired up. If the two sites are on opposite sublattices the only interaction is  $H_{J_1}^{(N)} = -\frac{J_1}{N} \sum_{\alpha\beta} |\alpha\alpha\rangle \langle \beta\beta|$  which can be shown to be unitary equivalent to Eq. (1) up to a constant. Between sites on the same sublattice we must have  $H_{J_2}^{(N)} = -\frac{J_2}{N} \sum_{\alpha\beta} |\alpha\beta\rangle \langle \beta\alpha|$ , studied in detail in [28] (for  $N = 2$  this is a ferromagnetic Heisenberg interaction between sites on the same sublattice). The effect of these two-spin terms on the imaginary time evolution of the basis states can be represented by the diagrams shown in Fig. 1(a), (b). It becomes clear that the quantum statistical mechanics of models in  $\mathcal{N}$ - $\tilde{\mathcal{N}}$  is equivalent to the classical statistical mechanics of specific tightly packed

loop models of  $N$  colors in one higher dimension. The staggered representations of  $\text{SU}(N)$  appear in the loop picture by requiring the orientation of a given loop to be such that it travels (in imaginary time) in opposite directions on opposite sublattices (if it travels up when its on an A site, it must always do so on all other A sites and it must always travel down when its on a B site; this property is illustrated for a 1-d system with  $J_1$  interactions in the Supplementary Materials (SM), Fig. 6).  $\text{SU}(N)$  invariant Hamiltonian operators must reconnect the loops without termination and preserve the directionality of the loops. Avoiding the sign problem only requires that the weight associated with a reconnection of loops be positive (this is Marshall’s sign condition).

Let us apply these ideas to design Marshall-positive four-spin Hamiltonian terms acting on the sites of an elementary plaquette. The simplest such connection is shown in Fig. 1(d), writing this as a Hamiltonian operator, it is  $H_Q^{(N)} = -\frac{Q}{N^2} \sum_{\alpha\beta\gamma\eta} (|\alpha\alpha\beta\beta\rangle \langle \gamma\gamma\eta\eta| + |\beta\alpha\alpha\beta\rangle \langle \eta\gamma\gamma\eta|)$  (the bra and kets are labeled by the spin indices at sites,  $ijkl$ ). It is easy to prove that for  $N = 2$  this interaction is unitarily equivalent to the  $Q$  term in Eq. (2). Interestingly, an independent four-spin interaction can be achieved by re-connecting the loops differently as shown in Fig. 1(e). In the bra-ket notation the new Hamiltonian is,

$$H_R^{(N)} = -\frac{R}{N^2} \sum_{\alpha\beta\gamma\eta} (|\alpha\alpha\beta\beta\rangle \langle \eta\gamma\gamma\eta| + |\beta\alpha\alpha\beta\rangle \langle \gamma\gamma\eta\eta|), \quad (3)$$

Written this way, the Marshall positivity of the  $R$ -term is obvious. We point out however that, unlike the  $Q$  term which is a product of two Marshall-positive  $J_1$  terms, in the usual language the  $R$  interaction’s positivity is non-trivial. Indeed, for  $N = 2$ , our new term may be written with familiar  $S = 1/2$  operators on each elementary plaquette (labeling the sites  $ijkl$  cyclically as shown in Fig. 1(a))

$$H_R^{(2)} = R \left( \left( \vec{S}_i \cdot \vec{S}_k - \frac{1}{4} \right) \left( \vec{S}_l \cdot \vec{S}_j - \frac{1}{4} \right) - \left( \vec{S}_i \cdot \vec{S}_l - \frac{1}{4} \right) \left( \vec{S}_k \cdot \vec{S}_j - \frac{1}{4} \right) - \left( \vec{S}_i \cdot \vec{S}_j - \frac{1}{4} \right) \left( \vec{S}_k \cdot \vec{S}_l - \frac{1}{4} \right) \right). \quad (4)$$

In contrast to the  $Q$ -term, the first term contains dot products between spins on sites *on the same* sublattice. Naively the first term would seem to make the  $R$ -interaction violate the Marshall rule, and indeed the first term *by itself* would. Remarkably however when all three terms of the  $R$ -interaction are taken together the offending matrix elements exactly cancel (after one does the usual Marshall rotation by an angle of  $\pi$  about the  $z$ -axis for the spins on one of the sublattices). We can re-

write the  $Q$  and  $R$  terms in a way in which their physics is more transparent,

$$\begin{aligned} H_Q^{(N)} &= -Q (|S_{ij}S_{kl}\rangle \langle S_{ij}S_{kl}| + |S_{il}S_{kj}\rangle \langle S_{il}S_{kj}|) \\ H_R^{(N)} &= -R (|S_{ij}S_{kl}\rangle \langle S_{il}S_{kj}| + |S_{il}S_{kj}\rangle \langle S_{ij}S_{kl}|) \end{aligned} \quad (5)$$

where  $|S_{ij}\rangle = \frac{1}{\sqrt{N}} \sum_{\alpha} |\alpha_i\alpha_j\rangle$  is the  $\text{SU}(N)$  singlet (refer to Fig. 1(a) for  $ijkl$  labeling). Now the physical

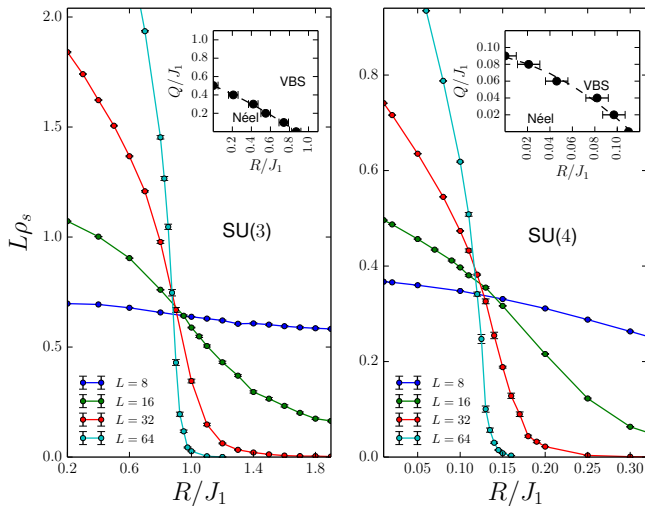


FIG. 2. Magnetic phase transitions from the crossing of  $\rho_s$  (stiffness) data shown for SU(3) and SU(4). In the main panels data for  $L\rho_s$  is shown for the  $J_1$ - $R$  model as a function of  $R/J_1$ . Clear evidence for a crossing is found which implies the existence of a critical point where magnetic order is destroyed. The insets show the magnetic phase boundaries for the  $J_1$ - $Q$ - $R$  model inferred from the kind of data shown in the main panel with  $Q \neq 0$  (not shown). We have chosen  $\beta = L$  and  $J_1 = 1$  here.

distinction between these two terms is apparent, see Fig. 1(f): The  $Q$ -interaction is a diagonal attractive term between two neighboring parallel singlet, whereas the  $R$ -interaction is an off-diagonal term that causes neighboring  $x$ -oriented singlets to become  $y$ -oriented singlets on an elementary plaquette. We note here that the  $Q$  and  $R$  are very reminiscent of the diagonal and off-diagonal terms respectively of the original quantum dimer model [29], but defined for spin models. Indeed in the  $N \rightarrow \infty$  mapping of the  $SU(N)$  antiferromagnet to the quantum dimer model [30], these are precisely the terms they would become.

The program can clearly be extended to systematically enumerate the 6-, 8-, or even higher spin interactions and can be carried out on any bipartite lattice by constructing loop reconfigurations of the kind shown in Fig. 1 (b-e) with the desired sets of sites. The study of this large family of Marshall positive Hamiltonians is an exciting direction for future work. In the remainder of this manuscript we present a study of the new  $R$  interaction.

*Numerical Simulations:* Since the  $J_1$ - $R$  model does not suffer from a sign problem we are able to study it on large system sizes and at low temperatures. Here we use the stochastic series expansion (SSE) method for which we have efficient loop updates for the quantum Monte Carlo [6].

It is well known that the  $J_1$  only model has Néel order for  $N = 2, 3, 4$  [14]. We first ask whether the new  $R$  interaction can destroy this Néel order in the  $J_1$ - $R$  model.

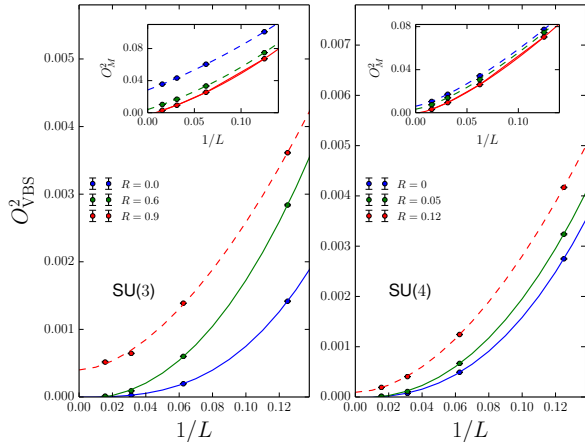


FIG. 3. Representative VBS (main panels) and magnetic (insets) order parameters for SU(3) and SU(4) for  $R = 0$  and on either side close to the critical points (the order parameters are defined in the SM). All fits through the QMC data points are shown only as a guide to the eye. The dashed (solid) lines correspond to cases where finite (zero) order parameters are obtained in the thermodynamic limit.

While this is not the case for  $N = 2$  (see Supplemental Materials), clear indications for crossings of  $\beta\rho_s = \langle W^2 \rangle$  (the average square of the winding number of the loops), which signal the destruction of magnetic order, are shown for SU(3) and SU(4) in Fig. 2. It has been previously shown that the  $Q$  interaction can also destroy the Néel order for  $N = 3, 4$ , giving rise to a VBS [24]. For completeness, the insets in Fig. 2 show the phase diagram of the  $J_1$ - $Q$ - $R$  model to connect our work with previous work on the  $J_1$ - $Q$  model.

The natural candidate for the large  $R$  non-magnetic state is a valence-bond solid. Finite-size scaling of the VBS and Néel order parameters ( $O_{\text{VBS}}$  and  $O_M$ ) close to the critical point confirm this expectation as shown in Fig. 3. The definition of the order parameters are standard, they are included in the SM for completeness. It is found that the Néel order parameters turn off at the same time the VBS order parameters first come on, consistent with the observation of such behavior in the  $J$ - $Q$  model [24] and with the deconfined criticality scenario [31]. An in depth study of the critical behavior is beyond the scope of the current work and will be presented elsewhere.

We note the VBS order parameter is finite in both the columnar and plaquette VBS states. It is now well established that the  $Q$  term favors columnar order [24], consistent with its interpretation as an attraction between neighboring parallel dimers. Since the  $R$  term appears to be more like the kinetic term in the dimer model (see Eq. (5) and discussion), it is interesting to ask what kind of VBS ordering the  $R$ -term favors. In order to make a

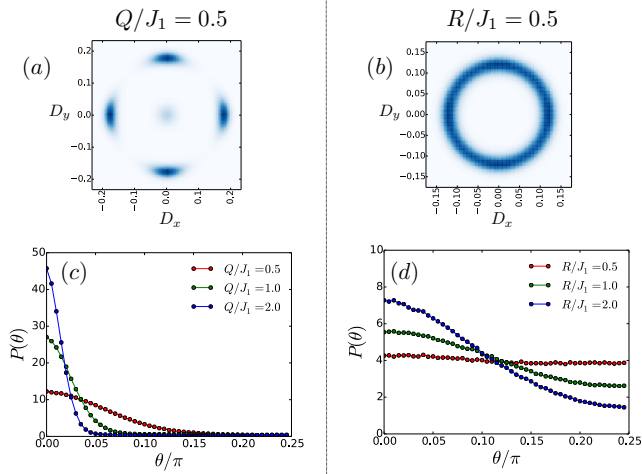


FIG. 4. Comparison and contrast of the VBS ordering in the  $J_1$ - $Q$  (left) and  $J_1$ - $R$  (right) model for  $SU(4)$ . (a,b) show 2- $d$  histograms of the VBS order parameter,  $D_y$  and  $D_x$ , measured at equal time on a  $64 \times 64$  systems at a coupling of  $Q/J_1 = 0.5$  and  $R/J_1 = 0.5$  (deep in the VBS phase for both models, see inset of right panel of Fig. 2 for phase diagrams). At the same couplings, the columnar nature of the ordering is much more apparent in the  $Q$  model as compared to the  $R$  model, where a  $U(1)$  symmetry is observed. (c,d) Showing the probability  $P(\theta)$  of getting a particular angle for the VBS order parameters on  $64 \times 64$  system for different couplings. By symmetry the function repeats itself in an eight-fold way and hence we show it only for  $0 < \theta < \pi/4$  (a half period). Note again the weak decay of  $P$  with  $\theta$  in the  $R$ -model, as compared to the  $Q$ -model. See text for discussion.

comparison of the two, we have studied both with the VBS histogram technique [16, 32]. A summary of our histogram study is shown in Fig. 4. For each configuration of our MC sample we can calculate the value of  $D_x$  (VBS order parameter with  $x$ -oriented dimers Fourier transformed to  $(\pi, 0)$ ) or  $D_y$  (analogously defined) – see SM for more details. A columnar VBS state should show a desire to be either only in  $D_x$  or only in  $D_y$  at a given time, whereas a plaquette VBS would show equal probability of being in both at any given time. We show data for the  $SU(4)$  case for which both  $Q$  and  $R$  destroy the magnetic order at a coupling ratio of order 0.1. So the data in Fig. 4 is deep in the VBS phase for both models. Consistent with this both systems show well formed valence bonds, as is clear by looking at the radius of the histograms in (a) and (b), though for an equally strong coupling the  $Q$  term has a larger amplitude. This weaker VBS order is also evident in the angular distribution. Here the  $Q$  terms shows very strong affinity for a columnar VBS with sharp peaks forming along the axis at  $(\pm D_x^0, 0)$  and  $(0, \pm D_y^0)$ , as shown in (c). In contrast, the  $R$  term admits a broad angular distribution even for large value of the  $R/J_1$  and big volumes (the data in (d) is shown for  $64 \times 64$ ). As  $R/J_1$  is increased even

further, there appears to be a trend towards a columnar VBS with increase of weight around  $\theta = 0$ , though as shown in Fig. 4 this crossover is very slow. This is somewhat surprising since both  $R$  and  $Q$  destroy Néel order at approximately the same value of the coupling. This new microscopic route to quantum criticality provided by the  $R$  term is an alternative to the well-studied  $J$ - $Q$  model and will be useful to test the independence from microscopic details of critical exponents and other putative universal quantities in future studies.

To conclude, we have introduced a systematic method to generate an infinitely large family of  $SU(N)$  Marshall positive Hamiltonians on bipartite lattice with multi-spin interactions. Many intriguing questions remain – How do we choose our coupling in this large parameter space to stabilize new phases of matter, *e.g.*, a spin liquid, in a sign-positive Hamiltonian? In what sense is the family of models we have found a complete set of Marshall positive models? Finally, as a practical application of our idea, we provided an alternate way to see the positivity of the popular  $Q$ -interaction, and discovered an independent positive four-spin  $R$ -term, which can be utilized as a new route to quantum criticality.

*Acknowledgements:* The author would like to thank T. C. Lang and A. W. Sandvik for stimulating discussions, J. Demidio for his help in preparing some figures, NSF DMR-1056536 for partial financial support and the BU visitor's program for their hospitality.

- 
- [1] H. A. Bethe, Z. Phys. **71** (1931).
  - [2] L. Balents, Nature **464**, 199 (2010).
  - [3] U. Schollwöck, Rev. Mod. Phys. **77**, 259 (2005).
  - [4] M. P. Gelfand and R. R. P. Singh, Advances in Physics **49**, 93 (2000), URL <http://www.tandfonline.com/doi/abs/10.1080/000187300243390>.
  - [5] N. Laflorencie and D. Poilblane, in *Quantum Magnetism* (Springer Berlin Heidelberg, 2004), vol. 645 of *Lecture Notes in Physics*, pp. 227–252, URL <http://dx.doi.org/10.1007/BFb0119595>.
  - [6] A. W. Sandvik, AIP Conf. Proc. **1297**, 135 (2010).
  - [7] P. Henelius and A. W. Sandvik, Phys. Rev. B **62**, 1102 (2000), URL <http://link.aps.org/doi/10.1103/PhysRevB.62.1102>.
  - [8] M. Nyfeler, F.-J. Jiang, F. Kämpfer, and U.-J. Wiese, Phys. Rev. Lett. **100**, 247206 (2008), URL <http://link.aps.org/doi/10.1103/PhysRevLett.100.247206>.
  - [9] A. Auerbach, *Interacting Electrons and Quantum Magnetism* (Springer, 1994).
  - [10] S. Bravyi, D. P. DiVincenzo, R. I. Oliveira, and B. M. Terhal, Quant. Inf. Comp. **8**, 361 (2008).
  - [11] R. K. Kaul, R. G. Melko, and A. W. Sandvik, Annu. Rev. Cond. Matt. Phys **4**, 179 (2013).
  - [12] I. Affleck, Phys. Rev. Lett. **54**, 966 (1985), URL <http://link.aps.org/doi/10.1103/PhysRevLett.54.966>.
  - [13] T. Nakamura and N. Hatano, Journal of the Physical Society of Japan **62**, 3062 (1993), URL <http://journals>.

- [jps.jp/doi/abs/10.1143/JPSJ.62.3062](https://jps.jp/doi/abs/10.1143/JPSJ.62.3062).
- [14] K. Harada, N. Kawashima, and M. Troyer, Phys. Rev. Lett. **90**, 117203 (2003).
  - [15] W. Marshall, Proc. R. Soc. London, Ser. A **232**, 48 (1955).
  - [16] A. W. Sandvik, Phys. Rev. Lett. **98**, 227202 (2007).
  - [17] R. G. Melko and R. K. Kaul, Phys. Rev. Lett. **100**, 017203 (2008).
  - [18] F. Jiang, M. Nyfeler, S. Chandrasekharan, and U. Wiese, J. Stat. Mech.: Theory and Experiment **2008**, 02009 (2008).
  - [19] K. Harada, T. Suzuki, T. Okubo, H. Matsuo, J. Lou, H. Watanabe, S. Todo, and N. Kawashima, Phys. Rev. B **88**, 220408 (2013), URL <http://link.aps.org/doi/10.1103/PhysRevB.88.220408>.
  - [20] A. W. Sandvik, Phys. Rev. Lett. **104**, 177201 (2010).
  - [21] A. Banerjee, K. Damle, and F. Alet, Phys. Rev. B **82**, 155139 (2010), URL <http://link.aps.org/doi/10.1103/PhysRevB.82.155139>.
  - [22] A. Sen and A. W. Sandvik, Phys. Rev. B **82**, 174428 (2010).
  - [23] S. Pujari, K. Damle, and F. Alet, Phys. Rev. Lett. **111**, 087203 (2013), URL <http://link.aps.org/doi/10.1103/PhysRevLett.111.087203>.
  - [24] J. Lou, A. W. Sandvik, and N. Kawashima, Phys. Rev. B **80**, 180414 (2009).
  - [25] R. K. Kaul, Phys. Rev. B **84**, 054407 (2011).
  - [26] A. Banerjee, K. Damle, and F. Alet, Phys. Rev. B **83**, 235111 (2011), URL <http://link.aps.org/doi/10.1103/PhysRevB.83.235111>.
  - [27] M. S. Block, R. G. Melko, and R. K. Kaul, *Fate of  $\mathbb{CP}^{N-1}$  fixed points with  $q$ -monopoles* (2013), URL <http://arxiv.org/abs/1307.0519>.
  - [28] R. K. Kaul and A. W. Sandvik, Phys. Rev. Lett. **108**, 137201 (2012).
  - [29] D. S. Rokhsar and S. A. Kivelson, Phys. Rev. Lett. **61**, 2376 (1988), URL <http://link.aps.org/doi/10.1103/PhysRevLett.61.2376>.
  - [30] N. Read and S. Sachdev, Nuclear Physics B **316**, 609 (1989), ISSN 0550-3213, URL <http://www.sciencedirect.com/science/article/pii/0550321389900618>.
  - [31] T. Senthil, A. Vishwanath, L. Balents, S. Sachdev, and M. Fisher, Science **303**, 1490 (2004).
  - [32] N. Kawashima and Y. Tanabe, Phys. Rev. Lett. **98**, 057202 (2007), URL <http://link.aps.org/doi/10.1103/PhysRevLett.98.057202>.



# SUPPLEMENTAL MATERIALS

Table I contains test comparisons between the energies obtained from a SSE-QMC study and exact diagonalization on  $4 \times 4$  and  $4 \times 6$  systems. Fig. 5 shows an approximate phase diagram of the SU(2)  $J_1$ - $Q$ - $R$  model.

size	$J_2$	$Q$	$R$	$\beta_{\text{QMC}}$	$E_{\text{ex}}$	$E_{\text{QMC}}$
$4 \times 4$	1	0	0	16	-1.164574932621	-1.16453(2)
$4 \times 4$	0	1	0	16	-1.547407628767	-1.54735(2)
$4 \times 4$	0	0	1	16	-1.532604539066	-1.53258(3)
$4 \times 4$	0	1	1	16	-2.395806575537	-2.39577(4)
$4 \times 4$	0	1	4	16	-4.947607904937	-4.94757(8)
$6 \times 4$	1	0	0	16	-1.144492865177	-1.14438(2)
$6 \times 4$	0	1	0	16	-1.51911890163	-1.51913(3)
$6 \times 4$	0	0	1	16	-1.50323567768	-1.50323(3)
$6 \times 4$	0	1	1	16	-2.349607914424	-2.34962(4)
$6 \times 4$	0	1	4	16	-4.847067604114	-4.84711(6)

TABLE I. Test comparisons of energies from exact diagonalization and finite- $T$  QMC studies for the SU(2) model. Note that  $J_1 = 1$  always. The energies reported here are per site and on square lattices with periodic boundary conditions.

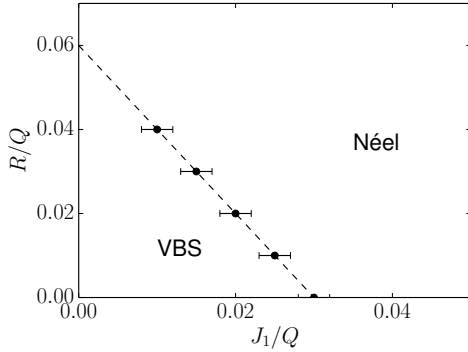


FIG. 5. An approximate phase diagram of the SU(2)  $J_1$ - $Q$ - $R$  model. This graph shows the location of the crossings of the size  $L = 16$  and  $L = 32$  data for  $L\rho_s$ . Similar to data shown in Fig. 2 but on smaller system sizes. It is well known that there are drifts in the critical point extracted from such crossings but that they eventually converge [17, 20], so this is an approximate representation of the phase diagram of the model. Nonetheless, this data shows that as opposed to the SU(3) and SU(4) cases discussed in the main manuscript, for SU(2) the  $R$  term alone does not destroy Néel order, in fact it seems to favor it! This is seen because at ratios of  $Q/J_1$  that give a VBS, increasing  $R$  drives the system back into the Néel phase.

We follow previous work [27] by defining an SU( $N$ )

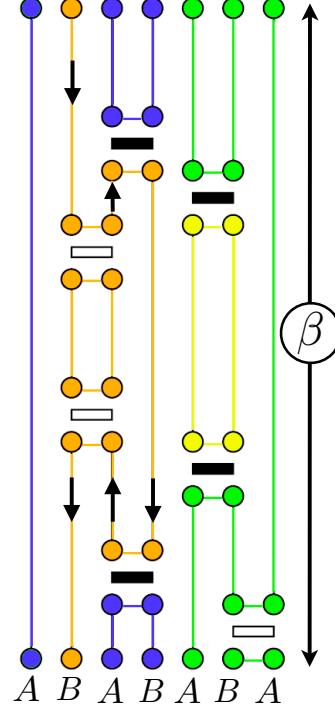


FIG. 6. An illustration of a path-integral or SSE contribution to the partition function of an SU( $N$ ) anti-ferromagnet with only  $J_1$  interactions with 7 sites at a temperature  $\beta$ , which may be viewed as a higher dimensional closed packed loop model. The orientation of one particular loop is followed with black arrows to show how it always travels in imaginary time in opposite directions on opposite sublattices (up on A and down on B). This orientation is preserved by the  $J_1$  interaction as well as all other SU( $N$ ) invariant interactions. An SU( $N$ ) antiferromagnet will have  $N$  different color assignments to the loops.

magnetic order parameter:

$$Q_{\alpha\beta}(\mathbf{r}, \tau) = \begin{cases} (|\alpha\rangle \langle \beta|)_{\mathbf{r}, \tau} - \delta_{\alpha\beta} \frac{1}{N} & , \text{ A sublattice} \\ (|\beta\rangle \langle \alpha|)_{\mathbf{r}, \tau} - \delta_{\alpha\beta} \frac{1}{N} & , \text{ B sublattice} \end{cases} \quad (6)$$

where  $\alpha$  and  $\beta$  vary over the  $N$  colors. We can then define a magnetic order parameter as:

$$O_M^2 \equiv \frac{1}{(N_s\beta)^2} \sum_{\mathbf{r}, \mathbf{r}'} \int_0^\beta d\tau \int_0^\beta d\tau' \langle T_\tau Q_{\alpha\beta}(\mathbf{r}, \tau) Q_{\beta\alpha}(\mathbf{r}', \tau') \rangle. \quad (7)$$

In a similar fashion we can define a VBS correlation function. First we define the bond operator on a pair of

nearest neighbor sites as follows:

$$B^\mu(\mathbf{r}, \tau) = \frac{1}{N} \mathcal{P}(\mathbf{r}, \tau; \mathbf{r} + \hat{\mu}, \tau), \quad (8)$$


---

where  $\mathcal{P}_{ij} = \sum_{\alpha, \beta=1}^N |\alpha\alpha\rangle_{ij} \langle\beta\beta|_{ij}$ , with spacetime locations of the two points given by the arguments. The superscript  $\mu$  denotes the bond type. On the square lattice this index would run over  $\mu = x, y$ . We can then study the correlations of these bond operators at different points in space and take the  $\omega = 0$  component:

$$C^{\mu\nu}(\mathbf{r} - \mathbf{r}') \equiv \frac{1}{\beta^2} \int_0^\beta d\tau \int_0^\beta d\tau' \langle T_\tau B^\mu(\mathbf{r}, \tau) B^\nu(\mathbf{r}', \tau') \rangle - \langle B^\mu \rangle \langle B^\nu \rangle. \quad (9)$$


---

The plaquette and columnar VBS patterns corresponds to a wavevector  $\mathbf{Q} = (\pi, 0)$  and correlated bond type  $\mu, \nu = x$ . By taking the Fourier component of at this wavevector, we can check for a signal in this VBS pattern. This is how we define our VBS order parameter:

$$O_{\text{VBS}}^2 \equiv \frac{1}{N_s} \sum_{\mathbf{r}} C^{xx}(\mathbf{r}) e^{i\mathbf{Q} \cdot \mathbf{r}}. \quad (10)$$

Finally to create the VBS histograms we take a basis state and assign 1 to all bonds which have same  $\text{SU}(N)$  colors on the sites that connect the bonds and 0 to all bonds connecting different colors. We then Fourier transform all the  $x$  directed bonds to  $(\pi, 0)$  and call this  $D_x$  and all the  $y$  directed bonds to  $(0, \pi)$  and call this  $D_y$ . This gives us a value of  $D_x$  and  $D_y$  for each basis state. We then histogram this data to get the density plots shown in Fig. 4.